

## Electrical conductivity as an indicator of iron reduction rates in abiotic and biotic systems

Aaron Regberg,<sup>1</sup> Kamini Singha,<sup>1,2</sup> Ming Tien,<sup>3</sup> Flynn Picardal,<sup>4</sup> Quanxing Zheng,<sup>4</sup> Jurgen Schieber,<sup>5</sup> Eric Roden,<sup>6</sup> and Susan L. Brantley<sup>1,2</sup>

Received 17 May 2010; revised 26 November 2010; accepted 20 December 2010; published 16 April 2011.

[1] Although changes in bulk electrical conductivity ( $\sigma_b$ ) in aquifers have been attributed to microbial activity,  $\sigma_b$  has never been used to infer biogeochemical reaction rates quantitatively. To explore the use of electrical conductivity to measure reaction rates, we conducted iron oxide reduction experiments of increasing biological complexity. To quantify reaction rates, we propose composite reactions that incorporate the stoichiometry of five different types of reactions: redox, acid-base, sorption, dissolution/precipitation, and biosynthesis. In batch experiments and the early stages of a column experiment, such reaction stoichiometries inferred from a few chemical measurements allowed quantification of the Fe oxide reduction rate based on changes in electrical conductivity. The relationship between electrical conductivity and fluid chemistry did not hold during the latter stages of the column experiment when  $\sigma_b$  increased while fluid chemistry remained constant. Growth of an electrically conductive biofilm could possibly explain this late stage  $\sigma_b$  increase. The measured  $\sigma_b$  increase is consistent with a model proposed by analogy from percolation theory that attributes the increased conductivity to growth of biofilms with conductivity of  $\sim 5.5 \text{ S m}^{-1}$  in at least 3% of the column pore space. This work demonstrates that measurements of  $\sigma_b$  and flow rate, combined with a few direct chemical measurements, can be used to quantify biogeochemical reaction rates in controlled laboratory situations and may be able to detect the presence of biofilms. This approach may help in designing future field experiments to interpret biogeochemical reactivity from conductivity measurements.

**Citation:** Regberg, A., K. Singha, M. Tien, F. Picardal, Q. Zheng, J. Schieber, E. Roden, and S. L. Brantley (2011), Electrical conductivity as an indicator of iron reduction rates in abiotic and biotic systems, *Water Resour. Res.*, 47, W04509, doi:10.1029/2010WR009551.

### 1. Introduction

[2] Microorganisms impact subsurface chemistry in ways that may affect fluid and bulk electrical conductivity  $\sigma_f$  and  $\sigma_b$  [Atekwana *et al.*, 2004a, 2004b, 2004c]. For instance, the study of an aquifer contaminated with hydrocarbons at the Crystal Refinery in Carson City, Michigan, revealed a zone of increased  $\sigma_b$  near the hydrocarbon-water interface that corresponds to increased microbial activity [Werkema *et al.*, 2003]. A conceptual model has been suggested to explain conductivity increases at contaminated sites [Sauck, 2000], and specific microbial processes like iron reduction, metha-

nogenesis, sulfate reduction, and sulfide oxidation have been identified [Allen *et al.*, 2007].

[3] To date, field-scale  $\sigma_b$  measurements have been difficult to interpret mechanistically because of the complicated nature of larger systems. Even laboratory measurements of  $\sigma_b$  in biogeochemical systems have been difficult to interpret. Bulk conductivity has been measured in biogeochemical systems containing environmental consortia (i.e., a culture containing all the bacterial species from a natural system) [Abdel Aal *et al.*, 2004; Davis *et al.*, 2006], and in some cases, additional electrical measurements of complex conductivity [Ntarlagiannis *et al.*, 2005; Abdel Aal *et al.*, 2009] and self-potential [e.g., Ntarlagiannis *et al.*, 2007] were collected to provide further insights. Despite this work, many unanswered questions remain regarding the effect of microbial growth and respiration on  $\sigma_b$  in natural systems and in laboratory experiments.

[4] In this paper we describe a series of simple experiments focusing on specific microbial processes to elucidate the effects of these processes on changes in chemistry,  $\sigma_f$  and  $\sigma_b$ . Specifically, we investigate if it is possible to quantify biogeochemical reaction rates from changes in electrical conductivity measured in systems with dissimilatory iron-reducing bacteria (DIRB). Dissimilatory iron-reducing organisms commonly impact subsurface water chemistry under the anoxic conditions associated with organic-contaminated

<sup>1</sup>Department of Geosciences, Pennsylvania State University, University Park, Pennsylvania, USA.

<sup>2</sup>Earth and Environmental Systems Institute, Pennsylvania State University, University Park, Pennsylvania, USA.

<sup>3</sup>Department of Biochemistry and Molecular Biology, Pennsylvania State University, University Park, Pennsylvania, USA.

<sup>4</sup>School of Public and Environmental Affairs, Indiana University, Bloomington, Indiana, USA.

<sup>5</sup>Department of Geological Sciences, Indiana University, Bloomington, Indiana, USA.

<sup>6</sup>Department of Geology and Geophysics, University of Wisconsin-Madison, Madison, Wisconsin, USA.

**Table 1.** Reaction Stoichiometries

Reaction Number	Type	Reaction
<i>Individual Reaction Types That Are Summed Into Composite Reactions</i>		
(R1)	Redox (metal reduction)	Reductant + MOOH → Oxidant + M <sup>2+</sup> + 2 OH <sup>-</sup>
(R2)	Acid-base <sup>a</sup>	H <sub>n</sub> A → mH <sup>+</sup> + H <sub>(n-m)</sub> A <sup>m-</sup>
(R3)	Sorption	≡SOH + M <sup>2+</sup> → ≡SOM <sup>+</sup> + H <sup>+</sup>
(R4)	Biosynthesis	0.05 NH <sub>4</sub> <sup>+</sup> + 0.125 CH <sub>3</sub> COO <sup>-</sup> + 0.075 H <sup>+</sup> → 0.05 C <sub>5</sub> H <sub>7</sub> O <sub>2</sub> N + 0.15 H <sub>2</sub> O
(R5)	Redox (methanogenesis)	0.125 CH <sub>3</sub> COO <sup>-</sup> + 0.125 H <sub>2</sub> O → 0.125 HCO <sub>3</sub> <sup>-</sup> + 0.125 CH <sub>4</sub>
(R6)	Dissolution/precipitation	M <sup>2+</sup> <sub>(aq)</sub> + HCO <sub>3</sub> <sup>-</sup> → MCO <sub>3(s)</sub> + H <sup>+</sup>
<i>Composite Reactions</i>		
(R7)	Abiotic	9 C <sub>6</sub> H <sub>8</sub> O <sub>6</sub> + 4 α-FeOOH <sub>(s)</sub> + H <sup>+</sup> → 4 Fe <sup>2+</sup> + 8 H <sub>2</sub> O + 7 C <sub>6</sub> H <sub>7</sub> O <sub>6</sub> <sup>-</sup> + 2 C <sub>6</sub> H <sub>6</sub> O <sub>6</sub>
(R8)	In vitro <sup>b</sup>	HCOO <sup>-</sup> + 2 α-FeOOH <sub>(s)</sub> + x ≡FeOH + (5-x) HL <sup>-</sup> → 4 H <sub>2</sub> O + (5-x) L <sup>2-</sup> + x ≡FeOFe <sup>+</sup> + CO <sub>2</sub> + (2-x) Fe <sup>2+</sup>
(R9)	In vivo <sup>b</sup>	HCOO <sup>-</sup> + 2 α-FeOOH <sub>(s)</sub> + x ≡FeOH + (5-x) HL <sup>-</sup> → 4H <sub>2</sub> O + (5-x) L <sup>2-</sup> + x ≡FeOFe <sup>+</sup> + CO <sub>2</sub> + (2-x) Fe <sup>2+</sup>
(R10)	Column <sup>b</sup>	CH <sub>3</sub> COO <sup>-</sup> + 2.32 α-FeOOH <sub>(s)</sub> + 0.044 NH <sub>4</sub> <sup>+</sup> + 0.0696 ≡SOH + 2.3048 HL <sup>-</sup> + 0.8616 HCO <sub>3</sub> <sup>-</sup> → 0.6 CH <sub>4</sub> + 0.2088 Fe <sup>2+</sup> <sub>(aq)</sub> + 2.0416 FeCO <sub>3(s)</sub> + 0.0696 ≡SOFe <sup>+</sup> + 0.044 C <sub>5</sub> H <sub>7</sub> O <sub>2</sub> N + 3.012 H <sub>2</sub> O + 2.3048 L <sup>2-</sup>

<sup>a</sup>H<sub>n</sub>A is the conjugate acid and H<sub>(n-m)</sub>A<sup>m-</sup> is the conjugate base, where *n* is the number of hydrogen atoms on acid and *m* is the number of hydrogen atoms released.

<sup>b</sup>Here *x* is the fraction of reduced iron [Fe(II) <sub>sorbed</sub>]/([Fe(II) <sub>sorbed</sub>]+[Fe(II) <sub>aqueous</sub>]) that sorbs to surfaces (denoted as ≡S or ≡Fe). L is HEPES (C<sub>8</sub>H<sub>18</sub>N<sub>2</sub>O<sub>4</sub>S) in batch experiments or PIPES (C<sub>8</sub>H<sub>18</sub>N<sub>2</sub>O<sub>6</sub>S<sub>2</sub>) in column.

aquifers [Christensen *et al.*, 2001]. Furthermore, DIRB are ubiquitous [e.g., Abrams and Loague, 2000; Bennett *et al.*, 2000; Scheibe *et al.*, 2006] because iron oxides are an abundant terminal electron acceptor [Christensen *et al.*, 2001]. We report experiments of increasing complexity from abiotic batch experiments to batch experiments using a pure culture of a DIRB (*Shewanella oneidensis* MR-1) to a column experiment. We chose to use a pure culture in the batch experiments for ease of interpretation. For the column experiment, we switched to an environmental consortium to better mimic natural systems.

[5] Our experiments were designed to build the capability to combine chemical measurements (e.g., pH and [Fe(II)]) from a limited number of locations with geophysical measurements of electrical conductivity to yield models of subsurface biogeochemical activity. Currently, understanding biogeochemical reactions in aquifers requires extensive sample collection at many locations (e.g., monitoring wells) followed by time-consuming laboratory analyses for each sample. In contrast, geophysical methods may provide data that can map out reactions over spatially broader zones. To quantify reaction rates, it will be necessary to attribute spatially integrated changes in electrical measurements to discrete changes in fluid chemistry. Here we demonstrate how inferred reaction stoichiometries (Table 1) can be used in increasingly complex experimental systems to determine reaction rates; this development should provide a framework for future research in natural systems.

[6] We demonstrate a link between changes in concentrations and electrical conductivity versus time in the batch experiments. We are able to convert a change in conductivity versus time into a change in concentration versus time, which can then be used to calculate a geochemical reaction rate. Similarly, in the column experiment, concentrations in effluent change with time and document reaction rate. Because of the spacing of electrodes in the column, the electrical measurements represent an average conductivity

of the entire volume. Early in the column experiment,  $\sigma_b$  correlates to effluent chemistry and can be converted to an inferred reduction rate for the column. At later times,  $\sigma_b$  is influenced by another process, hypothesized here to be bio-film growth, and no longer reflects iron oxide reduction rates.

## 2. Electrical Conductivity and Reaction Rates

[7] Below, we demonstrate how electrical conductivity methods are useful for measuring biogeochemical reaction rates. For a defined chemical reaction, the differential change in reaction extent  $d\xi$  is defined as a function of  $n_j$ , the moles of species *j*:

$$d\xi = \frac{dn_j}{\nu_j}, \quad (1)$$

where  $\nu_j$  is the stoichiometric coefficient of the reaction (>0 for products and <0 for reactants). The rate of the reaction *R* is defined at constant volume *V* as

$$R = \frac{d\xi}{dt} = \frac{V dC_j}{\nu_j dt}, \quad (2)$$

where  $C_j$  is the concentration of species *j* in the pore fluid (mol m<sup>-3</sup>). For species that are ions in solution, the following relation can be written to define  $\sigma_f$  (S m<sup>-1</sup>):

$$\sigma_f = F \sum_j |Z_j| C_j \mu_j, \quad (3)$$

where *F* is Faraday's constant (C mol<sup>-1</sup>) and  $Z_j$  and  $\mu_j$  (m<sup>2</sup> (V s)<sup>-1</sup>) are the charge and electrical mobility of ion *j*. Combining equations (2) and (3) yields

$$d\sigma_f = F \sum_j |Z_j| \mu_j dC_j = \frac{F}{V} \sum_j |Z_j| \mu_j \nu_j d\xi \quad (4)$$

$$R = \frac{d\sigma_f V}{dt F \sum_j \mu_j |Z_j| \nu_j} \cdot 1 \quad (5)$$

[8] Combining equations (2) and (5), separating variables, and integrating over time yields

$$C_j = C_j^0 + \frac{\nu_j}{F \sum_j \mu_j |Z_j| \nu_j} (\sigma_f - \sigma_f^0), \quad (6)$$

where  $C_j^0$  and  $\sigma_f^0$  are initial ion concentrations and fluid conductivity, respectively. Equation (5) can be used to calculate a chemical reaction rate from a change in  $\sigma_f$  if the stoichiometry of the reaction is known. As shown in equation (4), the change in  $\sigma_f$  is directly related to the change in reaction extent. Equation (6) demonstrates that the term  $\frac{\nu_j}{F \sum_j \mu_j |Z_j| \nu_j}$  will control the slope of a plot of  $\sigma_f$  versus concentration  $C_j$ .

[9] The bulk conductivity of a fluid-saturated porous medium  $\sigma_b$  can often be described as a function of  $\sigma_f$  with the following equation:

$$\sigma_b = a^{-1} \sigma_f \phi^m, \quad (7)$$

where  $\phi$  is porosity [e.g., Archie, 1942; Balberg, 1986]. Here  $a$  (generally varying from 0.62 to 3.5) and  $m$  (from 1.37 to 1.95) are empirical factors related to the extent of cementation and tortuosity. The primary assumption behind equation (7) is that the solid phase is nonconductive relative to the liquid phase. When this is the case,  $\sigma_b$  is expected to vary predictably as a function of  $\sigma_f$  according to equation (7). However, in some settings, especially in the presence of clays, the assumption of a single nonconductive solid phase may be incorrect. For such cases where  $\sigma_b$  does not vary with  $\sigma_f$  as described by equation (7), the expression is often modified to include a surface conductivity term  $\sigma_{\text{surf}}$ :

$$\sigma_b = a^{-1} \sigma_f \phi^m + \sigma_{\text{surf}}. \quad (8)$$

[10] The term  $\sigma_{\text{surf}}$  is sometimes attributed to the presence of clay coatings on grains or, at larger scales, the presence of shale in the porous media [Juhász, 1981; Sen and Goode, 1992; Revil and Glover, 1998]. Alternately, at the grain scale,  $\sigma_{\text{surf}}$  is attributed to conduction through the electrical double layer around mineral grains [e.g., Waxman and Smits, 1968; Juhász, 1981; Johnson et al., 1987; Schwartz et al., 1989; Revil and Glover, 1997; Revil et al., 1998].

[11] Another approach used to modify equation (7) is to assume the presence of two conductive phases with bulk electrical conductivities  $\sigma_1$  and  $\sigma_2$  contributing to  $\sigma_b$  [e.g., Glover et al., 2000]:

$$\sigma_b = \sigma_1 \chi_1^m + \sigma_2 \chi_2^p. \quad (9)$$

[12] Here  $\chi$  is the volume fraction of phase 1 or 2 and  $m$  and  $p$  are treated as fitting factors related to the tortuosities of phases 1 and 2, respectively. Notably, for both equations (8) and (9), conductivity terms are summed to describe  $\sigma_b$ . If surface conduction or secondary phases

become significant contributors to  $\sigma_b$ , then the interpretation of chemical reaction rates from changes in  $\sigma_b$  using equation (5) becomes difficult or impossible.

[13] One goal of this research is to identify criteria that describe when biogeochemical conditions are favorable for interpreting subsurface reaction kinetics from electrical conductivity measurements. With such a mechanistic understanding, geophysical measurements might be interpreted more accurately for field systems.

### 3. Laboratory Experiments

[14] We first conducted a series of abiotic, in vitro, and in vivo batch experiments to test the effect of iron oxide reduction on  $\sigma_f$  with as few reactions and confounding variables as possible. In each case, synthetic goethite (4.5 mg mL<sup>-1</sup>) [Cornell and Schwertmann, 2003] was reduced in reactors in triplicate. The goethite was synthesized in two batches, and the surface area was measured with a Micromeritics ASAP 2000 BET surface area analyzer. Each reactor was a continuously stirred 50 mL flask maintained at ambient temperature. The concentration of the electron donor was varied to change the reaction rate.

[15] Abiotic experiments contained 0.01 or 0.1 M ascorbic acid solution and goethite [Zinder et al., 1986]. In vitro experiments allowed exploration of biological Fe reduction catalyzed by bacterial cell membranes without the complication of live cells; experiments were conducted with aliquots of total membrane fraction (TM) from *Shewanella oneidensis* MR-1 (0.1 mg mL<sup>-1</sup>) with 0.001, 0.01, or 0.1 M Na formate as the reductant [Ruebush et al., 2006] in 100 mM 4-(2-hydroxyethyl)-1-piperazinethanesulfonic acid (HEPES) buffer (pH = 7) under a 5% H<sub>2</sub>-95% N<sub>2</sub> headspace. In vivo experiments were inoculated with 0.8 mg cells mL<sup>-1</sup> of *S. oneidensis* in buffered solution with 0.01 or 0.1 M Na formate as the reductant under non-growth conditions [Ruebush et al., 2006]. To inhibit cell growth, neither nitrogen nor phosphorus were added.

[16] For all batch experiments, pH was measured in situ. Aliquots of the slurry were collected every 20 min, filtered through a 0.2 μm filter, and analyzed for Fe(II) concentration, [Fe(II)<sub>(aq)</sub>], using ferrozine [Stokey, 1970; Violier et al., 2000]. Solid-associated (adsorbed and/or precipitated) Fe(II) was extracted by adding 100 μL of 2 N HCl to 300 μL of unfiltered slurry to obtain a final concentration of 0.5 N HCl. The resulting solution was immediately centrifuged at 13,200 rpm for 1 min to pellet the suspended solids. A 50 μL sample was removed from the supernatant for analysis with ferrozine [Lovley and Phillips, 1986]. Additionally,  $\sigma_f$  was measured every 10 min ( $\pm 0.0005$  S m<sup>-1</sup>) with an Orion conductivity cell and every minute with an IRIS Syscal Pro meter with four electrodes (Wenner array, 1 cm spacing) designed for field geophysical measurements. The Orion cell consists of a set of graphite electrodes embedded in plastic. In contrast, the geophysical electrodes consist of Ag/AgCl wire insulated such that only the tip of the wire is conductive. The  $\sigma_f$  measurements with either the Orion cell or the field instrument take <1 s to collect and involve injecting small amounts of current (~0.1 mA) into the solution. Changes in  $\sigma_f$  versus time were compared to changes in aqueous and adsorbed Fe(II) concentrations versus time and were used to calculate reaction rates.

[17] To scale up from the batch experiments, iron reduction rates were measured in a flow-through column experiment. The column reactor (20.3 cm long, 7.6 cm ID) was constructed from an acrylic tube with walls 1.27 cm thick packed with 1552 g of air-dried, sieved, iron mineral-bearing sediment (2 wt % Fe) from the subsurface at Oyster, Virginia [Penn *et al.*, 2001]. The sediment was not sterilized by autoclave or exposure to radiation to avoid alteration of the sediment mineralogy. The large aspect ratio and thick walls of this column preclude significant O<sub>2</sub> diffusion [Kjeldsen, 1993]. The effluent end of the column was loosely packed with glass wool to prevent the transport of fine particles out of the column. The sediment was mixed with a microbial inoculum of shallow subsurface sediment from Dorn Creek in Madison, Wisconsin (9:1 ratio by mass). Such an environmental consortium contains all the species present in the natural system and was used instead of a pure culture to mimic natural conditions. The initial effective porosity was 0.33 and was measured with a NaBr tracer by determining when 50% of the tracer had exited the column [Knutsson, 1966; Freeze and Cherry, 1979]. Sterile, anoxic, 1,4-Piperazinediethansulfonic acid (PIPES)-buffered artificial groundwater (PBAGW) with 1 mM acetate and <5 μM Fe(II)<sub>aq</sub> (hereafter [Fe(II)<sub>aq</sub>]<sub>in</sub>) was pumped at 2 mL h<sup>-1</sup> through Teflon tubing using a glass syringe pump. The PBAGW contains NaCl (0.15 g L<sup>-1</sup>), CaCl<sub>2</sub> (0.30 g L<sup>-1</sup>), MgCl<sub>2</sub>·6H<sub>2</sub>O (0.50 g L<sup>-1</sup>), KH<sub>2</sub>PO<sub>4</sub> (0.006 g L<sup>-1</sup>), NH<sub>4</sub>Cl (0.01 g L<sup>-1</sup>), NaHCO<sub>3</sub> (0.25 g L<sup>-1</sup>), PIPES (3.35 g L<sup>-1</sup>), trace elements, and vitamins. All effluent was collected daily in a N<sub>2</sub>-purged tube and analyzed for acetate concentration, [acetate]<sub>out</sub>, using high-performance liquid chromatography, for [Fe(II)<sub>aq</sub>]<sub>out</sub> using ferrozine, and for [NH<sub>4</sub><sup>+</sup>]<sub>out</sub> using *o*-phthalaldehyde [Holmes *et al.*, 1999]. The flow rate was confirmed by measuring the volume of effluent collected each day.

[18] A Ag/AgCl wire electrode inside a glass tube filled with KCl-saturated agar was inserted 3.8 cm into the center of the column at a point 2.96 cm from the inlet at the bottom. Three more identical electrodes were inserted every 4.8 cm along the rest of the column axis (Figure 1). Only the tips of the electrodes were designed to be conductive. These electrodes are adequately nonpolarizable and resistant to reaction [Vanhala and Soininen, 1995]. To make  $\sigma_b$  measurements, current  $I$  was injected across the outer two electrodes at large enough levels (0.1–0.2 mA) so that voltage could be measured across the inner electrodes but low enough to avoid inducing electrochemical reactions. We began these measurements on day 70, as the concentrations in the column effluent were approaching steady state. An IRIS Syscal R2E resistivity meter was used to measure the voltage twice daily. Each  $\sigma_b$  measurement takes <1 min. From the measured voltage  $V$ ,  $\sigma_b$  was calculated using Ohm's law,  $V = I/S$ , where  $S$  is conductance. A geometric factor  $K$  (m) was used to convert  $S$  (in Siemens) to  $\sigma_b$  (S m<sup>-1</sup>):

$$\sigma_b = K^{-1}S. \quad (10)$$

[19] Here  $K^{-1}$  for the column was calculated to equal 0.0936 m<sup>-1</sup> using COMSOL Multiphysics [COMSOL, 2008], a finite element analysis software package. Measurements of  $\sigma_b$  collected for the column experiment represent

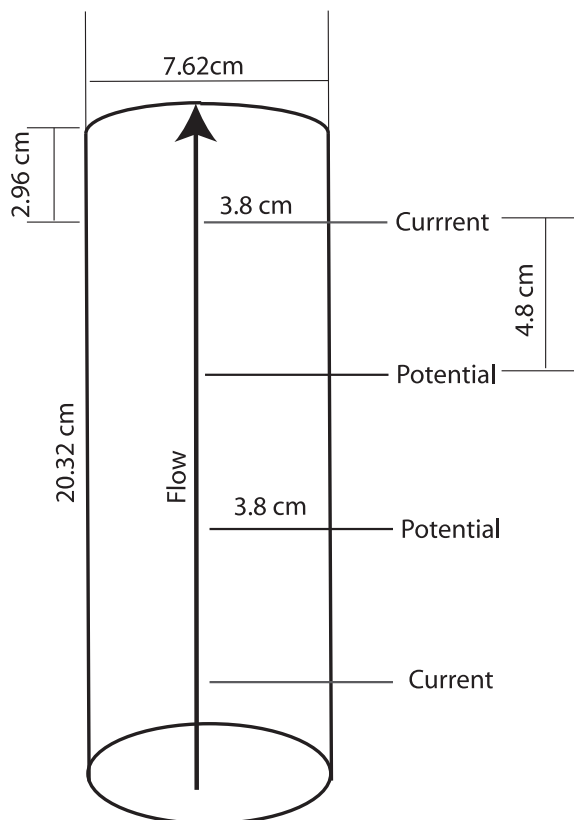
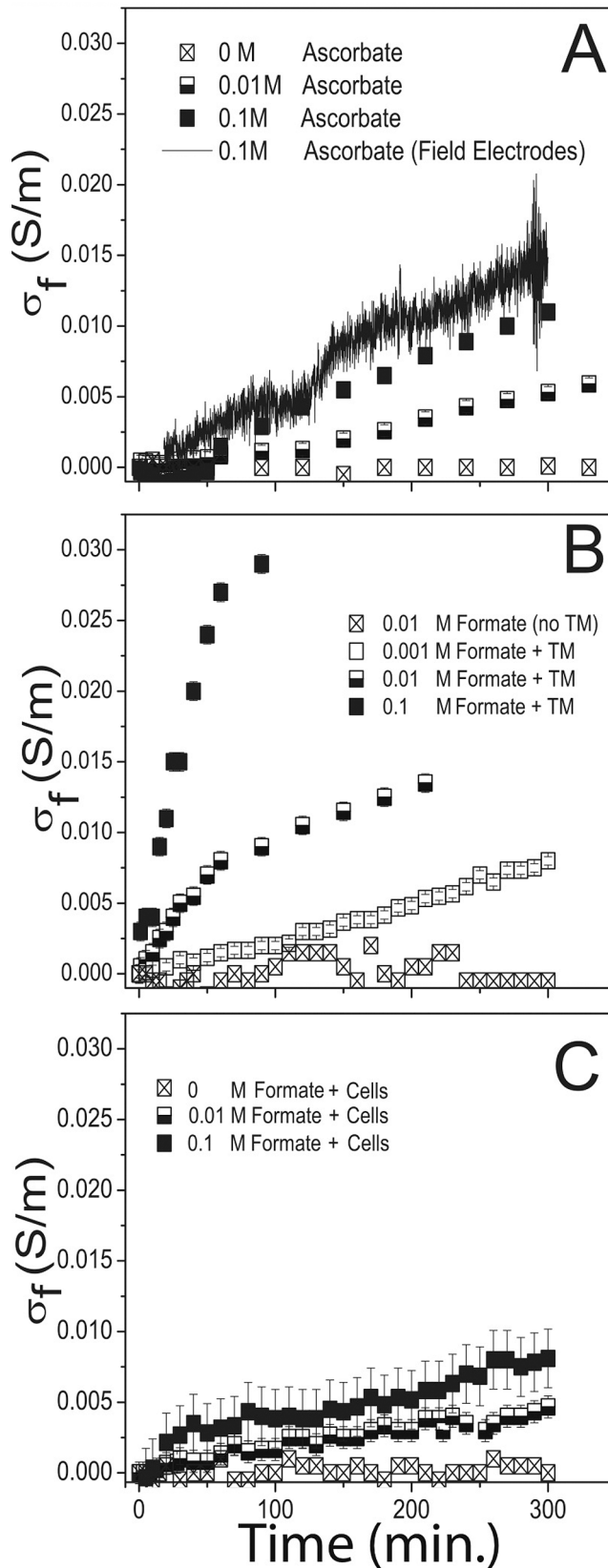


**Figure 1.** Schematic of the column reactor. Electrodes were Ag/AgCl wires encased in glass tubes and were only conductive at the tip.

a volume-weighted conductivity value over the area encompassed by the electrodes.

[20] At the conclusion of the experiment at 198 days, sediment was removed and examined with a FEI Quanta 400 FEG environmental scanning electron microscope (ESEM). Sediment samples were placed on 0.5 in. diameter Al sample stubs, allowed to air-dry for 30 min, and then immediately examined with scanning electron microscopy (SEM) under vacuum. All samples were examined in low-vacuum mode at 90 Pa chamber pressure. The operating voltage of the SEM was 15 kV. Samples were imaged simultaneously in secondary electron (SE) and backscatter electron (BSE) mode, and selected areas were also examined for elemental composition by energy dispersive X-ray spectroscopy (PGT Spirit EDS system).

[21] To extract sorbed Fe(II), 0.5 N HCl was incubated for 24 h with 10 g portions of the unwashed sediment from the top, bottom, and middle of the column following published experimental protocols [Heron *et al.*, 1994]. A separate analysis was also used to determine the amount of siderite and vivianite precipitation. In this latter extraction, the masses of CO<sub>2</sub>, Fe, Ca, Mg, and P released were measured after the reaction of 10 mL of 1 N HCl with 10 g of acetone-washed, postreaction column sediment for 24 h in a sealed vessel [White *et al.*, 1999]. It was assumed that all the Ca and Mg extracted with 1 N HCl was derived from solubilized carbonate minerals. The moles of CO<sub>2</sub> released were attributed to calcite and dolomite on the basis of the Ca and Mg concentrations in the 1 N HCl extraction, and



the remainder of the  $\text{CO}_2$  was attributed to siderite. A minor amount of excess Fe could be attributed to vivianite precipitation on the basis of the amount of P released. However, thermodynamic calculations performed with the geochemical speciation code PHREEQC using the default database [Parkhurst and Appelo, 1999] indicated that vivianite ( $\text{Fe}(\text{PO}_4)_2 \cdot 8 \text{H}_2\text{O}$ ) was undersaturated (Saturation Index =  $-0.23$ ); therefore, we assumed no vivianite precipitation. Any remaining Fe from the 1 N HCl extraction was considered as adsorbed onto mineral surfaces.

[22] Instantaneous Fe(II) release rates normalized to sediment surface area  $R_{\text{release}}$  ( $\text{mol Fe m}^{-2} \text{d}^{-1}$ ) were calculated as follows:

$$R_{\text{release}} = \frac{([\text{Fe}(\text{II})_{(\text{aq})}]_{\text{out}} - [\text{Fe}(\text{II})_{(\text{aq})}]_{\text{in}})Q}{AM}, \quad (11)$$

where  $Q$  is the flow rate ( $\text{L d}^{-1}$ ),  $A$  is the specific surface area of sediment ( $\text{m}^2 \text{g}^{-1}$ ), and  $M$  is the column sediment mass (g).  $[\text{Fe}(\text{II})_{(\text{aq})}]_{\text{in}}$  was observed to be below detection ( $\leq 5 \mu\text{M}$ ). As discussed in section 4.2, instantaneous Fe release rate can be calculated for aqueous Fe alone on the basis of equation (11) or a cumulative total release rate can be calculated from the sum of sorbed + aqueous + precipitated Fe(II),  $\text{Fe}(\text{II})_{\text{TOT}}$ :

$$\begin{aligned} R_{\text{release}}^{\text{total}} &= \frac{m\text{Fe}(\text{II})_{\text{TOT}}}{AMt} \\ &= \frac{(m\text{Fe}(\text{II})_{(\text{aq})\text{out}} + m\text{Fe}(\text{II})_{(\text{sorbed})} + m\text{Fe}(\text{II})_{(\text{siderite})})}{AMt}. \end{aligned} \quad (12)$$

[23] Here  $m$  is the cumulative moles of  $\text{Fe}(\text{II})_{\text{aq}}$  released from the column, the total Fe(II) sorbed, or total Fe(II) precipitated as siderite by the end of the experiment at time  $t = 298$  days. The specific surface area of the sediment  $A$  was set equal to  $\sim 1.48 \text{ m}^2 \text{g}^{-1}$  as measured in a previous study [Knapp et al., 2002].

**Figure 2.** Temporal evolution of measured fluid electrical conductivity ( $\sigma_f$ ,  $\text{S m}^{-1}$ ) during goethite reduction for (a) abiotic, (b) in vitro, and (c) in vivo batch experiments. All symbols represent data measured with the laboratory conductivity meter unless otherwise indicated. The initial increases in conductivity observed in the abiotic experiments were from  $1.18$  to  $4.25 \times 10^{-5} \text{ S min}^{-1}$ ; changes in vitro were in the range  $2.63$ – $37.6 \times 10^{-5} \text{ S min}^{-1}$ , while rates in vivo varied from  $2.0$  to  $3.0 \times 10^{-5} \text{ S min}^{-1}$ . Error bars indicate 1 standard deviation around the mean for replicate experiments; where no error bars are shown, standard deviations are smaller than symbols. In vitro rates were measured with fragments of the total membrane (TM) fraction of *Shewanella* cells as described in text, while in vivo rates were measured in the presence of cultures of *Shewanella*. No reduction was observed for controls without ascorbate (Figure 2a), TM (Figure 2b), or formate (Figure 2c). Note that  $\sigma_f$  was adjusted to plot at 0 for time 0 in each experiment.

## 4. Results

### 4.1. Batch Experiments

[24] Electrical conductivity measured with the field and laboratory electrodes in the batch experiments agreed within  $\pm 15\%$  (Figure 2a). The noise using the field instrumentation is attributed to small changes in electrode spacing caused by removing aliquots from the flask for chemical measurements. As expected, the laboratory instrument, with fixed electrode spacing, demonstrated better precision.

[25] Given the low reactivity of goethite, no change in  $\sigma_f$  was observed when the reductant was absent in the abiotic experiments; however, when ascorbate was present,  $\sigma_f$  increased with time, and the rate of increase accelerated with increasing concentration of ascorbate (Figure 2a). Note that in Figure 2 all experiments are plotted such that  $\sigma_f = 0$  at time 0; that is, the starting  $\sigma_f$  was subtracted from all subsequent  $\sigma_f$  measurements. The pH in the abiotic experiments started at 3.2 and increased to 4.6 at experiment termination.

[26] For in vitro and in vivo experiments, no conductivity change was observed, even in the presence of reductant (formate) unless TM or whole cells were present to catalyze the reaction (Figures 2b and 2c). When the reductant and catalyst were present,  $\sigma_f$  (Figure 2) and  $[\text{Fe(II)}_{\text{aq}}]$  (Figure 3) increased with time, and the rates of change in  $\sigma_f$  increased with greater concentrations of formate (Figures 2b and 2c). The pH remained constant in vitro and in vivo because of the presence of a HEPES buffer. At experiment termination, the concentration of sorbed Fe(II) per liter of solution was  $<1\%$ ,  $97\% \pm 3\%$ , and  $80\% \pm 2\%$  of the total  $[\text{Fe(II)}]$  for abiotic, in vitro, and in vivo experiments, respectively (Table 2).

### 4.2. Column Experiment

[27] In the column experiment,  $[\text{Fe(II)}_{\text{(aq)}}]_{\text{in}}$  was below detection ( $\leq 5 \mu\text{M}$ ), and  $[\text{Fe(II)}_{\text{(aq)}}]_{\text{out}}$  increased to a steady state value of  $0.18 \text{ mM}$  by day 50. The release rate at day

50 was equal to  $8.64 \mu\text{mol Fe(II)}_{\text{aq}} \text{ d}^{-1}$  and was equivalent to  $R_{\text{release}} = 0.0038 \pm 0.0002 \mu\text{mol Fe(II)}_{\text{aq}} \text{ m}^{-2} \text{ d}^{-1}$  (equation (11) and Figure 4).

[28] Measured  $[\text{acetate}]_{\text{out}}$  decreased below detection ( $\leq 0.05 \text{ mM}$ ) after day 75 (Figure 4), consistent with a steady state instantaneous consumption rate of  $\leq 39.1 \mu\text{mol acetate d}^{-1}$ .  $[\text{NH}_4^+]_{\text{out}}$  also attained steady state values ( $0.16 \text{ mM}$ ) at day 75, consistent with an instantaneous consumption rate of  $1.8 \mu\text{mol NH}_4^+ \text{ d}^{-1}$  (Figure 4). Acetate consumption is necessary for microbial respiration and growth. In contrast,  $\text{NH}_4^+$  consumption only occurs for cell growth. Cell growth into biofilms is consistent with observations by SEM on the reacted sediments that revealed carbon-rich coatings (Figure 5).

[29] At the conclusion of the experiment, the average of the  $0.5 \text{ N HCl}$  extractable Fe(II) for four samples was  $7.61 \pm 0.59 \text{ mmol}$  (equivalent to  $0.0049 \text{ mmol g}^{-1}$  sediment). There was a noticeable trend in the  $0.5 \text{ N HCl}$  extractable Fe(II) measured in these four samples. Sediment samples collected along the length of the column showed a decrease in concentration from  $0.0067 \text{ mmol Fe(II) g}^{-1}$  sediment at  $4 \text{ cm}$  from the inlet to  $0.0063 \text{ mmol Fe(II) g}^{-1}$  sediment at  $8 \text{ cm}$  from the inlet to  $0.0030 \text{ mmol Fe(II) g}^{-1}$  sediment at  $12 \text{ cm}$  from the inlet to  $0.0050 \text{ mmol Fe(II) g}^{-1}$   $16 \text{ cm}$  from the inlet. These values were corrected for the initial concentration in sediment, observed to equal  $0.001 \text{ mmol Fe(II) g}^{-1}$ . The average value of all four samples is reported in Table 2.

[30] At the conclusion of the experiment,  $16.45 \pm 0.002 \text{ mmol sorbed } \pm \text{ precipitated Fe(II)}$  (equivalent to  $0.0106 \text{ mmol g}^{-1}$  sediment) were extracted with  $1 \text{ N HCl}$ . Of this total,  $1.4 \pm 5.16 \text{ mmol}$  of Fe(II) were attributed to sorbed Fe(II) on the basis of the argument described in the next paragraph. Within 2 standard deviations this value was the same as the  $\text{Fe(II)}_{\text{sorbed}}$  measured in the  $0.5 \text{ N}$  extraction ( $7.61 \pm 0.59 \text{ mmol}$ ). The  $0.5 \text{ N HCl}$  probably extracted some siderite [Heron *et al.*, 1994] also.

[31] The  $1 \text{ N HCl}$  extraction released  $39 \mu\text{mol CO}_2 \text{ g}^{-1}$  sediment (equivalent to  $60.5 \text{ mmol CO}_2$  for the entire reactor). Of this,  $46.1 \text{ mmol}$  were attributed to Mg and Ca carbonates (on the basis of Ca and Mg measurements in the extractant), and the remaining  $14.4 \pm 5.16 \text{ mmol}$  of  $\text{CO}_2$  were attributed to siderite. However, this extraction released  $16.45 \text{ mmol Fe}$ , leaving  $2.05 \text{ mmol noncarbonate Fe}$ . Since we calculated vivianite to be undersaturated, we did not include it in our mass balance. Therefore, the remaining  $2.05 \pm 5.16 \text{ mmol}$  of Fe(II) was present as sorbed Fe(II). No siderite or vivianite were detected in fresh sediment before the experiment.

[32] On the basis of these data, a total of  $18.10 \text{ mmol}$  of Fe (released  $\text{Fe}_{\text{aq}} + 1 \text{ N HCl}$  extracted Fe) were reduced over 198 days. This includes the cumulative release of aqueous Fe(II) determined by summing the mass of Fe(II) in each sample, i.e.,  $1.653 \text{ mmol}$  over 198 days. Therefore, of the  $18.10 \text{ mmol}$  of Fe reduced,  $>90\%$  was retained in the column. These values are equivalent to  $91.4 \mu\text{mol Fe(II)}_{\text{TOT}} \text{ d}^{-1}$  or  $0.0398 \mu\text{mol Fe}_{\text{TOT}} \text{ m}^{-2} \text{ d}^{-1}$  of reduction, assuming a constant reduction rate over the entire experiment (equation (12)).

[33] Similarly, the cumulative consumption of acetate was determined to be  $8.08 \text{ mmol}$  by summing the mass of acetate in each outlet sample and subtracting this value

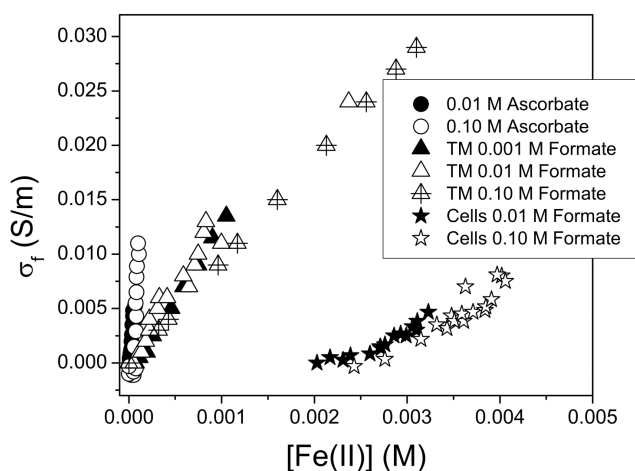


**Figure 3.** Fluid electrical conductivity  $\sigma_f$  increases as  $[\text{Fe(II)}_{\text{aq}}]$  increases in abiotic (circles), in vitro (triangles), and in vivo (stars) batch experiments. The slope of  $\sigma_f$  ( $\text{S m}^{-1}$ ) versus  $[\text{Fe(II)}_{\text{aq}}]$  is a reflection of the reaction stoichiometry of each type of experiment (see equation (6)). In all cases,  $\sigma_f$  measured at the start of the experiment has been corrected to start at 0.

**Table 2.** Experimental Conditions and Results<sup>a</sup>

	Abiotic	In Vitro	In Vivo	Column
Starting (influent) pH	3.2	7.55	7.50	~7
Final (effluent) pH	4.6	7.59	7.55	~7
Electron donor	Ascorbic acid C <sub>6</sub> H <sub>8</sub> O <sub>6</sub>	Formate HCOO <sup>-</sup>	Formate HCOO <sup>-</sup>	Acetate CH <sub>3</sub> COO <sup>-</sup>
Electron acceptor	α-FeOOH	α-FeOOH	α-FeOOH	Ferric oxide
Buffer	Ascorbic acid	HEPES	HEPES	PIPES
Atmosphere	Air	N <sub>2</sub> (95%) H <sub>2</sub> (5%)	N <sub>2</sub> (95%) H <sub>2</sub> (5%)	Ar
[Electron donor] <sup>b</sup>	0.01 (3), 0.1 (3)	0.001 (3), 0.01 (3), 0.1 (3)	0.01 (3), 0.1 (3)	0.001 (1)
Percent Fe adsorbed <sup>c</sup>	<1%, <1%	97% ± 3%, 97% ± 3%, 97% ± 3%	81% ± 6%, 78% ± 2%	11% ± 2%
Percent Fe precipitated <sup>c</sup>	NA	NA	NA	80%
Surface area (m <sup>2</sup> g <sup>-1</sup> )	19.3, 19.3	25.4, 19.3, 19.3	25.4, 25.4	1.48
d[Fe(II)]/dt <sup>d</sup>	0.1, 0.3	5.8, 9.5, 29.5	2.7, 4.3	NA
dσ <sub>f</sub> /dt <sup>e</sup>	1.18, 4.25	2.63, 10.5, 37.6	2.0, 3.0	NA
Rate based on [Fe(II) <sub>aq</sub> ] <sup>f</sup>	0.10, 0.30	10.4, 18.5, 43.5	4.8, 7.6	0.0038
Rate based on σ <sub>g</sub> <sup>g</sup>	0.12, 0.44	7.1, 23.1, 57.5	6.2, 9.9	0.0041

<sup>a</sup>Rates calculated over the entire 5 h batch experiments or steady state portion of column experiment. NA indicates not applicable.

<sup>b</sup>Molar. For each experiment, the number of replicates is shown in parentheses.

<sup>c</sup>Batch experiments:  $[\text{Fe(II)}_{\text{sorbed}}]/([\text{Fe(II)}_{\text{sorbed}}] + [\text{Fe(II)}_{\text{aq}}])$  as calculated at the end of experiment. Column experiments:  $\text{mol Fe(II)}_{\text{sorbed}}/(\text{mol Fe(II)}_{\text{sorbed}} + \text{mol Fe(II)}_{\text{aq}})$ .

<sup>d</sup>Rate  $\times 10^{-6} \text{ M min}^{-1}$ ;  $[\text{Fe(II)}] = [\text{Fe(II)}]_{\text{aq}} + [\text{Fe(II)}]_{\text{adsorbed}}$  for batch experiments.

<sup>e</sup>Batch experiments ( $d\sigma_f/dt \times 10^{-3} \text{ S m}^{-1} \text{ min}^{-1}$ ).

<sup>f</sup>Abiotic, nmol m<sup>-2</sup> min<sup>-1</sup>; in vitro and in vivo, nmol (mg TM)<sup>-1</sup> m<sup>-2</sup> min<sup>-1</sup>; column,  $\mu\text{mol m}^{-2} \text{ d}^{-1}$ .

<sup>g</sup>Rate based on σ<sub>f</sub> and equation (5) for abiotic (nmol m<sup>-2</sup> min<sup>-1</sup>) and for in vitro and in vivo (nmol (mg TM)<sup>-1</sup> m<sup>-2</sup> min<sup>-1</sup>) experiments but based on σ<sub>b</sub> and equations (5) and (7) for column experiments ( $\mu\text{mol m}^{-2} \text{ d}^{-1}$ ) from day 70 to 120.

from the total mass of acetate introduced to the column over the entire experiment. This corresponds to a cumulative acetate consumption rate of 40.8  $\mu\text{mol d}^{-1}$ . Note that this value is very similar to the instantaneous acetate consumption rate calculated previously from effluent chemistry and flow rate.

[34] Influent σ<sub>f</sub> equaled 0.276 S m<sup>-1</sup> throughout the experiment, and steady state effluent σ<sub>f</sub> after day 70 equaled 0.281 S m<sup>-1</sup>, as calculated from measured ionic concentrations. In contrast, measurements of σ<sub>b</sub> across the column remained constant ( $\sim 0.055 \text{ S m}^{-1}$ ) only from day 70 to 120, but after day 120, σ<sub>b</sub> began to increase to  $\sim 0.18 \text{ S m}^{-1}$  (Figure 4). The ionic strength of the effluent remained constant at 26 mM during this increase in σ<sub>b</sub>.

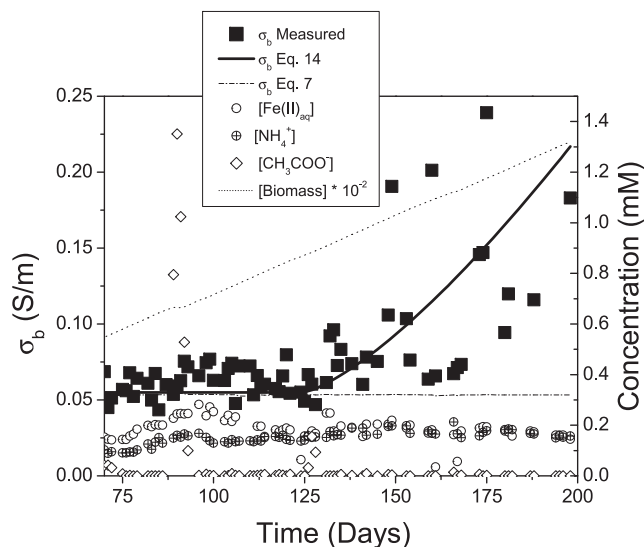


**Figure 4.** Values of measured  $\sigma_b$  (squares) plotted versus time for the column experiment. Also shown are measured effluent concentrations of  $\text{NH}_4^+$  (crossed circles), acetate (open diamonds), and  $\text{Fe(II)}_{\text{aq}}$  (open circles). Biomass concentration  $\times 10^{-2}$  is also plotted versus time (dotted line) as calculated from the cumulative consumption of acetate and ammonia and reaction (R10) in Table 1. Dash-dotted line indicates  $\sigma_b$  calculated from equation (7) on the basis of known effluent chemistry. Solid line indicates  $\sigma_b$  calculated from equation (14) as described in the text.

## 5. Discussion

[35] The intent of this research was to develop an approach to interpret field measurements of electrical conductivity in terms of biogeochemical reaction rates. This is an inverse problem and will yield nonunique, model-derived reaction rates that must be constrained by chemical measurements. With these chemical measurements, the reaction stoichiometries can be identified, allowing interpretation of the geophysical data. We demonstrate this general approach hereafter. Reaction models will be iteratively proposed and tested against measured conductivity until discrepancies between the model predictions and the measured data are minimized. Here we iterate by using investigator-written geochemical models; however, inverse modeling modules in geochemical codes such as PHREEQC can also be used [Parkhurst and Appelo, 1999] to constrain more complicated field systems.

[36] For the batch experiments, composite reaction stoichiometries (numbered reactions in Table 1) were proposed and used to compare the measured values of  $d\sigma_f/dt$  to measured concentrations using equations (5) and (6). It is easy to see that the batch experiments (abiotic, in vitro, and in vivo) have different stoichiometries describing different reactions by comparing the slopes of the lines in Figure 3. The relationship between σ<sub>f</sub> and Fe(II) is different for each experimental condition. Different reactions were tested until a stoichiometry was found that fit the observed rate of change in conductivity and the measured chemistry. For

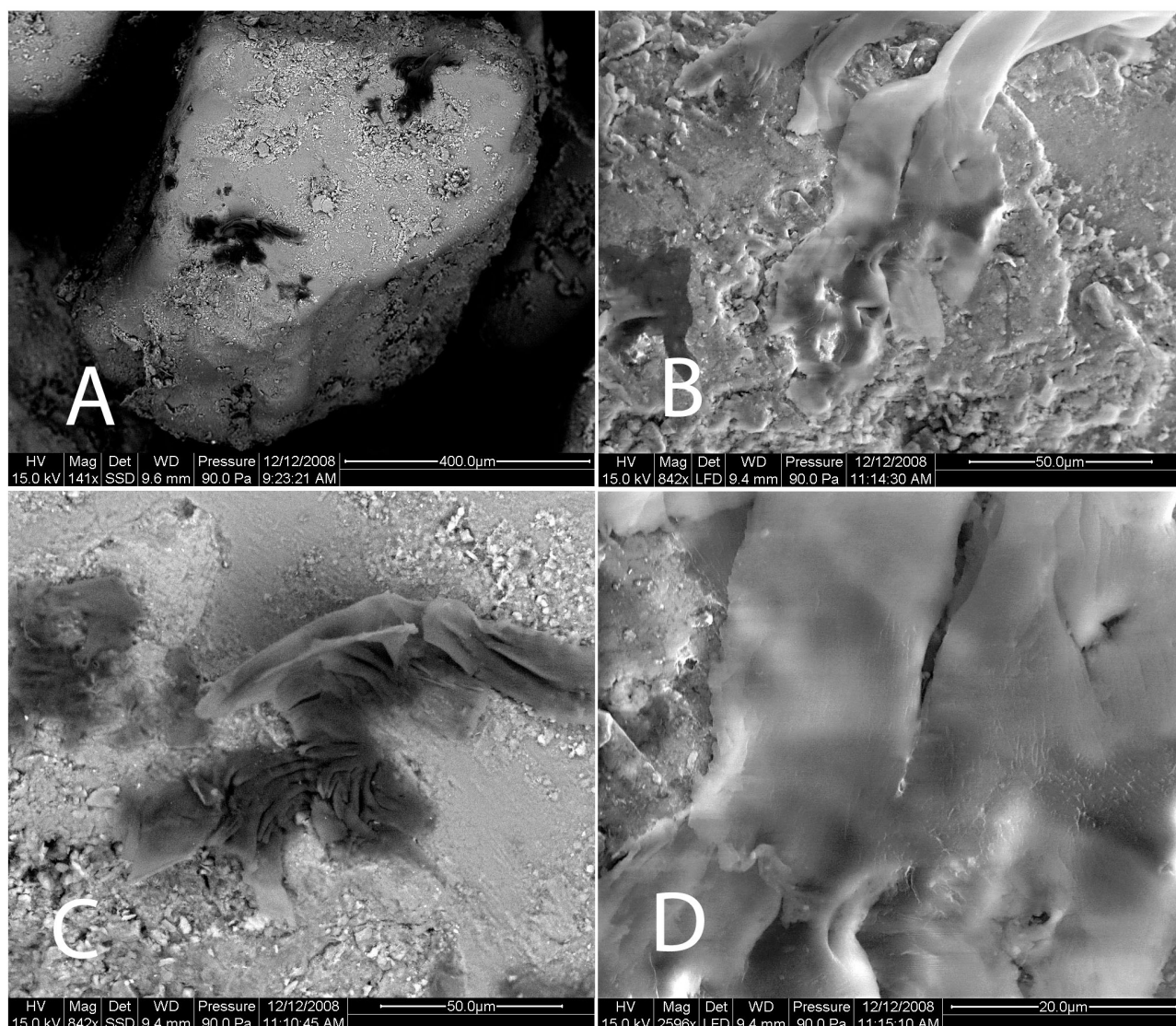
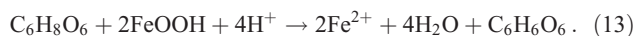


**Figure 5.** Scanning electron microscope images of biofilm patches on sediment grains from the column experiment. (a) In backscattered electron mode, biofilms appear as dark patches because of the high carbon content and low molecular weight. Enlargements of the (b, d) upper and (c) lower patches reveal the surface texture of the biofilms.

example, in the abiotic batch experiment, the stoichiometry of the redox reaction (reaction (R1) in Table 1) incorporating ascorbic acid ( $C_6H_8O_6$ ) oxidation and goethite reduction was initially written as follows:



[37] Given that the initial pH of the experiments (pH = 3.2) was less than the pKa of ascorbic acid [Kumler and Daniels, 1935], pKa = 4.12, no deprotonation of ascorbic acid was included in the proposed reaction. However, the stoichiometry of equation (13) is inconsistent with the change in  $\sigma_f$  as documented in Figure 6a. This inconsistency led us to conclude that an additional acid-base reaction (reaction (R2) in Table 1) was missing from equation (13). Furthermore, the pH values of the abiotic experiments increased from starting values of 3.2–4.6 at experiment termination, well above the pKa of ascorbic acid. When the

appropriate acid-base reaction for ascorbic acid was added to equation (13), reaction (R7) in Table 1 was the result. Using reaction (R7), the calculated changes in  $\sigma_f$  from measured changes in ionic concentrations for the abiotic experiments were similar to the measured increases in  $\sigma_f$  (Figure 6b). Importantly, we did not need to make measurements of the ascorbate ion concentrations once the reaction stoichiometry was inferred from the slope of Figure 6a. Consistency is demonstrated in Figure 6b, where the measured conductivity is plotted along with the summed contributions of conductivities for all ions. Using equation (5) and the stoichiometry from reaction (R7) (Table 1), the calculated reduction rate from measured values of  $d\sigma_f/dt$  is  $0.12 \text{ nmol Fe(II) m}^{-2} \text{ min}^{-1}$  for the  $0.01 \text{ M}$  ascorbic acid experiment, consistent with a reduction rate from measured values of  $d[Fe(II)_{aq}]/dt$  of  $0.10 \text{ nmol m}^{-2} \text{ min}^{-1}$  as summarized in Table 2 (ionic mobilities summarized in Table 3). Sorption in these abiotic experiments was <1%,

as measured with a 0.5 N HCl extraction. This is consistent with a pH value of  $<4.5$ .

[38] In contrast to these abiotic experiments, the pH was  $>7$  in the in vitro and in vivo experiments, and sorption was significant. Therefore, composite reactions used to interpret in vitro and in vivo data had to include a reduction reaction (reaction (R1) in Table 1), an acid-base reaction (reaction (R2) in Table 1), and a sorption reaction (reaction (R3) in Table 1). Chemical measurements to determine the extent of Fe(II) adsorption were also necessary. With measured adsorption, composite reactions (R8) and (R9) were written.

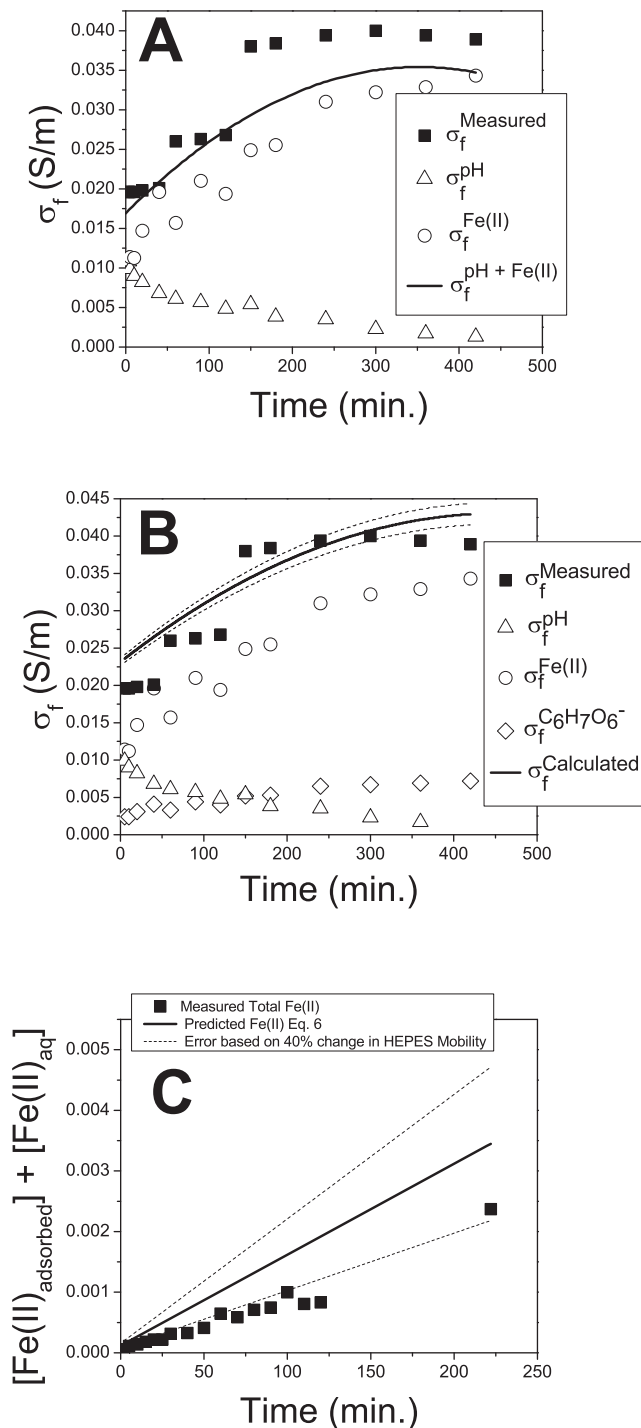


**Table 3.** Ionic Diffusion Constants and Mobilities

Ion	Diffusion Constant ( $\text{m}^2 \text{s}^{-1} \times 10^{-5}$ )	Mobility <sup>a</sup> ( $\text{m}^2(\text{V s})^{-1} \times 10^{-7}$ )
H <sup>+</sup>	9.311	3.626
Fe <sup>+3</sup>	1.812	2.117
Fe <sup>+2</sup>	1.438	1.120
OH <sup>-</sup>	5.273	2.053
CHO <sub>2</sub> <sup>-</sup> (formate)	1.454	0.566
HCO <sub>3</sub> <sup>-</sup>	1.185	0.461
CO <sub>3</sub> <sup>2-</sup>	1.846	1.438
Na <sup>+</sup>	1.334	0.519
Cl <sup>-</sup>	2.032	0.791
K <sup>+</sup>	1.957	0.762
Ca <sup>+2</sup>	1.584	1.234
Mg <sup>+2</sup>	1.424	1.100
C <sub>8</sub> H <sub>17</sub> N <sub>2</sub> O <sub>4</sub> S <sup>-</sup> (HEPES)	0.554	0.431
C <sub>8</sub> H <sub>17</sub> N <sub>2</sub> O <sub>6</sub> S <sub>2</sub> <sup>-</sup> (PIPES)	0.467	0.364
CH <sub>3</sub> CO <sub>2</sub> <sup>-</sup> (acetate)	1.089	0.424
NH <sub>4</sub> <sup>+</sup>	1.957	0.762
C <sub>6</sub> H <sub>7</sub> O <sub>6</sub> <sup>-</sup> (ascorbate)	0.687	0.267
C <sub>6</sub> H <sub>6</sub> O <sub>6</sub> (dehydroascorbic acid)	0.692	0.269

<sup>a</sup>Ion mobilities are from published values [Landolt-Bornstein, 1969] or estimated from diffusion constants [Schwarzenbach et al., 2003].

For example, in the in vitro experiment, a measured change in  $\sigma_f$  can be converted to a change in Fe(II) concentration using equation (6). A change in  $\sigma_f$  is partitioned to changes in the relevant ionic species (in this case Fe(II), HCO<sub>3</sub><sup>-</sup>, and HEPES anion) using stoichiometry from reaction (R8). Using this method, the inferred rate of change of total Fe(II) based on measured changes in  $\sigma_f$  matched measured changes in total Fe(II) within error (equation (5); see Table 2 and Figure 6c). Error in the in vitro and in vivo experiments was primarily because of uncertainty surrounding the ionic mobility for the HEPES anion.

[39] With this inverse approach, the batch experiments were described within error with composite reactions (R7), (R8), and (R9) that summed redox (reaction (R1)), acid-base (reaction (R2)), and sorption (reaction (R3)) reactions. We were able to predict biogeochemical reaction rates from changes in  $\sigma_f$  in these well-constrained systems. The same approach was then pursued to interpret the column

**Figure 6.** (a, b) Measured  $\sigma_f$  (squares) versus time compared to calculated values (lines) during abiotic reduction of goethite by ascorbate. In Figure 6a, the line sums the contributions to  $\sigma_f$  calculated from changes in measured pH (triangles) and  $[\text{Fe(II)}]_{\text{aq}}$  (circles) only. Calculated values differ slightly from measured values ( $R^2 = 0.855$ ) because of ascorbate speciation, which is neglected in the calculations. A better estimate for  $\sigma_f$  ( $R^2 = 0.947$ ) is shown in Figure 6b when [ascorbate] (diamonds) is included assuming composite reaction (R7) (Table 1). (c) Comparison of measured (squares) or calculated (line)  $[\text{Fe(II)}]_{\text{tot}}$  for the in vitro experiment (for one replicate with 0.01 M Na formate) versus time. The calculated value is based on reaction (R8) (Table 1). Ion mobilities were derived from published values [Landolt-Bornstein, 1969] or estimated from diffusion constants [Schwarzenbach et al., 2003] (see Table 3). Dashed lines (Figures 6b and 6c) represent  $\pm 1$  standard deviation in this estimate. Background  $\sigma_f$  measured before experiments was subtracted for Figures 6a and 6b.

experiment. To create a composite reaction that describes the column experiment (reaction (R10)), additional reactions occurring in the column were included as described in section 5.1.

### 5.1. Interpreting the Column Experiment

[40] In addition to reactions (R1), (R2), and (R3) in Table 1 the composite reaction for the column must also incorporate biomass growth. Since  $\text{NH}_4^+$  and acetate consumption are both at steady state after day 70, the biomass growth rate was inferred to be constant after that point as well. Biomass growth in the column was estimated from acetate and ammonium consumption rates using the concept of yield coefficients  $\gamma$  [Rittmann and McCarty, 2001]. Every mole of  $\text{C}_5\text{H}_7\text{O}_2\text{N}$  (a generic formula for biomass) consumes 2.5 mol of acetate and 1 mol of N. However, the observed ratio of  $\text{NH}_4^+$  to acetate consumption was 0.05, much less than the 0.4 required by this stoichiometry. This is expected because most of the acetate was oxidized and converted to  $\text{HCO}_3^-$  during dissimilatory iron reduction. Assuming  $\text{NH}_4^+$  is only consumed by biomass growth, the ratio obtained by dividing the ammonia consumption rate (mol  $\text{NH}_4^+$   $\text{d}^{-1}$ ) by the acetate consumption rate (mol acetate  $\text{d}^{-1}$ ) is related to the growth yield  $\gamma$ . The growth yield expresses the relative partitioning of electrons from the electron donor into two sinks, new biomass and the terminal electron acceptor (in this case ferric iron), and can theoretically have a value between 0 and 1. In the column experiment,  $\gamma = 0.12$  on the basis of rates of  $\text{NH}_4^+$  consumption divided by the steady state instantaneous acetate consumption rate ( $\gamma = 1.8 \mu\text{mol NH}_4^+ \text{d}^{-1} / (39.1 \mu\text{mol acetate d}^{-1} \times 0.4)$ ).

[41] However, the observed rate of Fe reduction is not consistent with these interpretations. Specifically, if Fe(III) is the only terminal electron acceptor and assuming 8 el released per mole of acetate oxidized, then  $8(1 - \gamma)$  mol of Fe(II) are produced per mole of acetate consumed (Table 1, reaction (R1)). In contrast, the observed ratio of the rate of Fe(III) reduction ( $91.4 \mu\text{mol d}^{-1}$ ) to the cumulative acetate consumption rate ( $40.8 \mu\text{mol d}^{-1}$ ) is too low, consistent with a higher growth yield of  $\gamma = 0.72$ . This value is inconsistent with literature values for growth yields:  $\gamma = 0.12 - 0.15$  for growth of *Geobacteraceae* species on amorphous Fe(III) oxides [Lovley and Phillips, 1988; Roden and Lovley, 1993; Caccavo et al., 1994].

[42] Therefore, another process in addition to Fe reduction and biomass production was inferred to consume acetate. Mass balance dictates that the cumulative consumption of acetate released 64.6 meq el. Iron reduction accounts for 28% of the 61.9 meq el released (on the basis of the summed total of  $\text{Fe}_{(\text{aq})}(\text{II})_{\text{out}} + 1 \text{ N HCl extractable Fe(II)}$ ), and biomass production accounts for another 12% (on the basis of the mass of  $\text{NH}_4^+$  consumed and the stoichiometry in reaction (R4) in Table 1). The remaining 60% of electrons released from acetate could have produced methane if methanogenesis (reaction (R5) in Table 1) occurred in the column. Methanogenesis is the only reasonable respiration pathway in this system given that no additional ionic solutes were measured in the column effluent.  $\text{HCO}_3^-$  produced via methanogenesis presumably precipitated as siderite. The column was effectively impermeable to  $\text{O}_2$  diffusion inward from the atmosphere, and so  $\text{O}_2$  is not a reasonable sink for

electrons released from acetate [Kjeldsen, 1993]. Reactions for biomass growth and methanogenesis were added to the composite reaction (see reaction (10)) on the basis of these arguments.

[43] Thermodynamic calculations with PHREEQC [Parkhurst and Appelo, 1999] are consistent with chemical oversaturation of siderite in the effluent by day 50. Furthermore, extractions with 1 N HCl were also consistent with the presence of siderite. The composite reaction that includes Fe(III) reduction, acid-base buffering, Fe(II) sorption, methanogenesis, biomass growth, and siderite precipitation (reaction (R10) in Table 1) is consistent with the relative changes in concentrations of all measured species between influent and effluent. On the basis of the cumulative consumption of acetate and using reaction (R10) in Table 1, biomass production was calculated as a function of time and plotted in Figure 4.

### 5.2. Conductivity

[44] For the column experiment, measured values of  $\sigma_b$  were compared to  $\sigma_f$  using equation (7). To do this, we assumed values of  $a$  within the range of 0.63–3.5 and  $m$  within the range of 1.37–1.95 on the basis of literature values [e.g., Archie, 1942; Balberg, 1986]. Values of  $\sigma_b$  calculated from equation (7) and effluent chemistry with  $a = 1$  and  $m = 1.5$  were consistent with measured  $\sigma_b$  before day 120. Furthermore, the Fe(II) release rate calculated from measured  $\sigma_b$ ,  $0.0041 \mu\text{mol Fe(II)}_{\text{aq}} \text{m}^{-2} \text{d}^{-1}$ , using equations (5) and (7) and composite reaction (R10) (Table 1), is consistent with the rate calculated from the measured  $[\text{Fe(II)}_{\text{aq}}]$  ( $0.0038 \mu\text{mol Fe(II)}_{\text{aq}} \text{m}^{-2} \text{d}^{-1}$ ) in effluent from day 70 to 120 using equation (11). As described for the batch experiments, we are able to calculate Fe(II) reduction rates from changes in  $\sigma_b$  before day 120 in the column.

[45] However, after day 120,  $\sigma_b$  increased by a factor of 3 (Figure 4), while measured effluent chemistry did not change significantly. The cause of this  $\sigma_b$  increase that is unrelated to changes in effluent chemistry is not readily apparent. It is unlikely that methane bubbles formed within the column experiment or affected  $\sigma_b$ . The solubility of methane at 298 K under 1 atmosphere of pressure is about  $35 \text{ mg L}^{-1}$  (2.47 mM) [Duan and Mao, 2006]. The methane concentration was calculated from the flow rate ( $0.048 \text{ L d}^{-1}$ ) and the cumulative acetate consumption rate ( $40.8 \text{ mmol d}^{-1}$ ) assuming 0.60 mol methane produced per mole acetate (composite reaction (R10) in Table 1). The calculated methane concentration, 0.510 mM, was well below saturation. Furthermore, any gas bubbles that did form would be less conductive than the pore fluid, and their presence would temporarily decrease the measured  $\sigma_b$  [Knight, 1991; Wang et al., 2000; Serra and Serra, 2005]. Methane bubbles cannot explain the  $\sigma_b$  increase.

[46] This result is surprising because deviation from equation (7) is sometimes associated with conductive minerals and the known Fe(II) precipitate siderite is generally non-conductive [Rzhevskii et al., 1965]. There are several other possible explanations for the measured increase in  $\sigma_b$  after day 120. Changes in porosity could affect electrical conductivity; however,  $\phi$ ,  $a$ , or  $m$  would be required to change to unreasonable values of 0.87, 0.34, or 0.81 to match observations (see equation (7)). It is impossible to keep all three

parameters within acceptable bounds and still describe the measured increase in  $\sigma_b$ .

[47] If geochemical gradients exist within the column, it is possible that they are affecting  $\sigma_b$ . For example, a change in  $[\text{Fe(II)}_{\text{aq}}]$  or sorbed Fe(II) along the length of the column could affect surface conductance and thus  $\sigma_b$ . However, the gradient in sorbed Fe(II) as documented by our HCl extractions reported earlier is presumed to have been present, along with a gradient in  $\text{Fe(II)}_{\text{aq}}$ , from relatively early in the experiment and would not have caused changes in  $\sigma_b$  starting at day 120.

[48] In literature treatments, when measured  $\sigma_b$  is above the value predicted from fluid chemistry alone using equation (7), most conductivity models have been expanded to include either a surface conductivity term or a term for a secondary conductive phase as in equation (8) or (9). For example, *Atekwana et al.* [2004b] used a variable surface conductivity term ( $\sigma_{\text{surf}} = 1\text{--}10 \text{ mS m}^{-1}$ ; equation (8)) to explain discrepancies between  $\sigma_b$  and  $\sigma_f$  in measurements in a borehole that passed through a zone of hydrocarbon contamination above an aquifer in Carson City, Michigan. They attributed the surface conductivity to changes in the electrical double layer around mineral surfaces caused by microbial activity. However, they did not present chemical or physical data such as measured changes in ionic strength, surface roughness, or cation exchange capacity to support their hypothesis. *Slater et al.* [2009] took a conceptually different approach by modeling conductivity data with a parallel conductivity term that is mathematically similar to surface conductivity. The authors noticed an increase in  $\sigma_b$  measured in a flow-through column containing Se-reducing bacteria while effluent  $\sigma_f$  remained constant. *Slater et al.* [2009] were able to fit their data by adding a second conductivity term, similar to the surface term in equation (8), with variable values between 2 and  $12 \text{ mS m}^{-1}$ . They referred to their new term as a parallel conductivity path.

[49] The largest changes in  $\sigma_b$  measured in our column can be modeled using equation (8) with  $\sigma_{\text{surf}}$  equal to about  $127 \text{ mS m}^{-1}$ . It is unlikely that this addition is because of a change in surface conductivity with time, however, because changes in surface conductivity are generally small when ionic strength is held constant. Similar to *Slater et al.* [2009], we attribute the  $\sigma_b$  increase in our column not to a surface conductivity but to a new, parallel, conductive pathway. The ionic strength in the column remained relatively constant throughout the experiment, increasing by only 0.75% (26.6 versus 26.8 mM) despite extensive dissolution of iron oxides. Surface conductivity stops being affected by changes in ionic strength above 10 mM [*Revil and Glover*, 1997]; therefore, it is unlikely that we have developed significant surface conductivity.

[50] The concept of surface conductivity as described above is an unlikely explanation for increased  $\sigma_b$ , but it is possible that ferrous iron sorbed onto ferric oxide surfaces creates a unique type of surface conductivity that is not explicitly accounted for in previous publications [e.g., *Revil and Glover*, 1997]. Previous research has demonstrated that adsorbed ferrous iron is capable of transferring electrons onto ferric oxides [e.g., *Tronc et al.*, 1984; *Icopini et al.*, 2004; *Williams and Scherer*, 2004; *Crosby et al.*, 2005; *Handler et al.*, 2009]. While it is possible that this

electron transfer affects macroscopic conductivity, no one has demonstrated this phenomenon conclusively. During our column experiment, the mass of adsorbed iron increased, but the total mass of iron inside the column decreased by 16%. For these reasons we believe that ferrous sorption onto ferric oxides is not causing the  $\sigma_b$  increase measured in the column experiment.

[51] In contrast to the decrease in total Fe in the column, the biomass grew in the column even after day 120. It is possible that this steady increase in biomass could increase surface conductivity by increasing the total surface area within the column. Increasing the surface area of a sample can increase its cation exchange capacity which in turn increases surface conductivity [e.g., *Revil and Glover*, 1998]. However, the sediment in the column had an initial surface area of  $2300 \text{ m}^2$  ( $= 1.48 \text{ m}^2 \text{ g}^{-1} \times 1552 \text{ g}$ ). Approximately  $4.4 \times 10^{12}$  cells were produced during the entire experiment on the basis of a  $\gamma$  value of 0.12 calculated as described previously (mass of 1 cell assumed to equal  $1 \times 10^{-12} \text{ g}$  [*Sundararaj et al.*, 2004]). If each cell has an average surface area of  $6 \times 10^{-12} \text{ m}^2$ , then the total increase in surface area because of biomass production is  $26 \text{ m}^2$ , which is 1% of the total surface area inside the column. A 1% increase in surface area is unlikely to produce significant increases in cation-exchange capacity, and surface conductance since biomass has a similar sorption capacity to iron oxide minerals [*Urrutia et al.*, 1998].

[52] Since the effect of iron sorption and biomass growth on surface conductivity is unlikely to be significant, we consider the possibility that cells connecting into biofilms by day 120 create a new conductive phase and cause a dramatic  $\sigma_b$  increase (Figure 4). While we cannot confirm that biofilms are conductive, we use a theoretical approach to consider how the electrical conductivity of microbial biofilms might impact this experiment. This conceptual model is based on the assumptions about microbial growth from cumulative acetate and  $\text{NH}_4^+$  consumption discussed above. The model does not require a massive increase in biomass after day 120. Instead, we hypothesize that day 120 represents the point at which a threshold is crossed such that sufficient numbers of discrete patches of biofilm become connected across the column. SEM analyses of the sediments reveal biofilm-like coatings on mineral grains (Figure 5). While the column effluent was at steady state, the rate of biomass growth did not change. However, the amount of biomass connectivity was presumably increasing.

[53] Because  $\sigma_b$  shows a threshold-type behavior (Figure 4), we propose a theoretical model based on percolation theory to describe  $\sigma_b$  increases. This is only one of many possible ways to model the effect of biofilm growth and connectivity but is a first step in considering how biofilms might explain this data set. Percolation theory has been used to describe changes in hydraulic conductivity, microorganism populations, and other properties [e.g., *Kirkpatrick*, 1973; *Deutsch*, 1989; *Thullner et al.*, 2002]. It incorporates a threshold that depends on the volume fraction of a new phase, assumed to be biomass in this case. By analogy to *Deutsch's* equation for hydraulic conductivity and equation (9),  $\sigma_b$  is assumed to follow equation (7) until the fraction  $f_{\text{secondary}}$  of secondary material with higher conductivity  $\sigma_{\text{secondary}}$  exceeds a critical

fraction  $f_{\text{critical}}$ , at which point a new term appears in the equation:

$$\sigma_b = a^{-1} \sigma_f \phi^m + (f_{\text{secondary}} - f_{\text{critical}})^\omega \sigma_{\text{secondary}}. \quad (14)$$

[54] For hydraulic conductivity, the geometry of permeable zones is thought to control the values of  $f_{\text{critical}}$  and  $\omega$  ( $1.5 < \omega < 2$ ) [Deutsch, 1989]. Interestingly,  $\omega$  in equation (14) may be similar to  $p$  in equation (9) since both values can be attributed to tortuosity effects.

[55] As argued,  $f_{\text{critical}}$  describes the critical volume fraction of biomass. Assuming a constant  $\gamma$  of 0.12 and the cumulative consumption of acetate, we calculated  $f_{\text{secondary}}$  for the volume fraction of biomass from the moles of  $\text{C}_5\text{H}_7\text{O}_2\text{N}$ , average cell volume ( $1 \times 10^{-9} \text{ mm}^3$ ), cell mass ( $3.0 \times 10^{-7} \mu\text{g}$ ) [Sundararaj et al., 2004], reactor volume ( $920 \text{ cm}^3$ ), and porosity (0.33). The calculated value of  $f_{\text{secondary}}$  at 120 days, i.e.,  $\sim 3\%$ , was assumed equal to  $f_{\text{critical}}$ . Fitting the data to equation (7) for  $f_{\text{secondary}} < f_{\text{critical}}$  before 120 days and to equation (14) for values above  $f_{\text{critical}}$  after day 120 yields  $\sigma_{\text{secondary}} = 5.5 \text{ S m}^{-1}$  if  $\omega = 1.5$  (Figure 4). According to our hypothesis, this is an estimate for the conductivity of respiring biofilm in the reactor.

[56] These  $\sigma_{\text{secondary}}$  values for a biofilm, approximately 20 times that of  $\sigma_f$ , are reasonable. Many mechanisms might cause electrical conductivity in a biofilm. For example, it is well known that most soil bacteria can produce extracellular polymeric substances that affect hydrologic as well as chemical conditions in and around biofilms [e.g., Little et al., 1991; Or et al., 2007]. Furthermore, Liermann et al. [2000] demonstrated that  $[\text{H}^+]$  in biofilms grown on Fe-containing minerals is up to 10X higher than in the bulk fluid, and Marsili et al. [2008] have argued for electron shuttles in biofilms. Either of those species in biofilms could increase conductivity. Nanowires could also contribute to biofilm conductivity if they are present [e.g., Reguera et al., 2005; Ntarlagiannis et al., 2007; Nielsen et al., 2010], but nanowires are not a prerequisite for a conductive biofilm. Torres et al. [2008] calculated a conductivity  $\geq 0.05 \text{ S m}^{-1}$  in biofilms, and Ramasamy et al. [2008] observed a 40% decrease in kinetic impedance as biofilms grew inside fuel cells. As mentioned earlier, the analogous but much smaller increase in conductivity measured across a column containing Se(IV)-reducing bacteria [Slater et al., 2009] was also attributed to biofilm growth, although without chemical evidence to eliminate other explanations such as changes in pore fluid chemistry.

## 6. Implications and Conclusions

[57] Our observations have implications for interpreting  $\sigma_b$  in microbially active sediments. For example, in the aquifer in Carson City, Michigan,  $\sigma_b$  varied by  $0.025 \text{ S m}^{-1}$  with depth [Atekwana et al., 2004b]. Using techniques outlined herein, a few colocated chemical and  $\sigma_b$  measurements versus depth could constrain composite reactions and be used to infer reaction rates using published approaches for interpreting chemistry versus depth in subsurface flow systems [e.g., Bau et al., 2004]. However, if  $\sigma_b$  becomes decoupled from  $\sigma_f$ , reaction rates would be difficult to determine. Indeed, Atekwana et al. inferred that something other than ionic solutes contributed to  $\sigma_b$  because they needed to set  $\sigma_{\text{surf}} = 10 \text{ mS m}^{-1}$  with equation (8) to describe the

Carson City aquifer. Our work provides a framework for further investigations of the effect of biofilm growth on  $\sigma_b$ .

[58] We suggest that models for biogeochemical reaction rates can in some cases be quantified using electrical conductivity and composite reaction stoichiometries but not in those instances where thresholds in conductivity are crossed that necessitate the modification of Archie's law. We propose a simple theoretical model that attributes a change in  $\sigma_b$  in our column experiments to a threshold that is crossed because of the increase in biomass. This research lays the groundwork for future investigations by presenting an iterative method that can be used to determine whether systems are above or below a threshold. More work on the electrical properties of biofilms is clearly needed. Future directions for this work include monitoring microbial activity and/or chemical changes associated with contaminant plumes, enhanced oil recovery, and  $\text{CO}_2$  sequestration.

[59] **Acknowledgments.** The authors acknowledge National Science Foundation grants CHE-0431328 to S. L. Brantley and M. Tien for the Center for Environmental Kinetics Analysis at Penn State and EAR-0525069 to Flynn Picardal as well as Department of Energy grant DE-FG02-08ER64520 to K. Singha and S. L. Brantley. An NSF equipment grant to J. Schieber (EAR-0318769) provided funds for the purchase of the FEI Quanta 400 FEG ESEM that was used for acquiring the images used in this paper. We acknowledge three extremely helpful reviews as well as discussions with D. Ross, T. Fischer, J. Nuester, L. Liermann, and J. Zachara.

## References

- Abdel Aal, G. Z., E. A. Atekwana, L. D. Slater, and E. A. Atekwana (2004), Effects of microbial processes on electrolytic and interfacial electrical properties of unconsolidated sediments, *Geophys. Res. Lett.*, *31*, L12505, doi:10.1029/2004GL020030.
- Abdel Aal, G., E. Atekwana, S. Radzikowski, and S. Rossbach (2009), Effect of bacterial adsorption on low frequency electrical properties of clean quartz sands and iron-oxide coated sands, *Geophys. Res. Lett.*, *36*, L04403, doi:10.1029/2008GL036768.
- Abrams, R., and K. Loague (2000), A compartmentalized solute transport model for redox zones in contaminated aquifers: 2. Field-scale simulations, *Water Resour. Res.*, *36*, 2015–2030, doi:10.1029/2000WR900110.
- Allen, J. P., E. A. Atekwana, E. A. Atekwana, J. W. Duris, D. D. Werkema, and S. Rossbach (2007), The microbial community structure in petroleum-contaminated sediments corresponds to geophysical signatures, *Appl. Environ. Microbiol.*, *73*, 2860–2870.
- Archie, G. E. (1942), The electrical resistivity log as an aid in determining some reservoir characteristics, *Trans. Am. Inst. Min. Metall. Pet. Eng.*, *146*, 54–62.
- Atekwana, E., E. Atekwana, F. Legall, and R. Krishnamurthy (2004a), Field evidence for geophysical detection of subsurface zones of enhanced microbial activity, *Geophys. Res. Lett.*, *31*, L23603, doi:10.1029/2004GL021576.
- Atekwana, E., E. Atekwana, R. Rowe, D. Werkema, and F. Legall (2004b), The relationship of total dissolved solids measurements to bulk electrical conductivity in an aquifer contaminated with hydrocarbon, *J. Appl. Geophys.*, *56*, 281–294.
- Atekwana, E. A. E., E. A. Atekwana, D. Werkema, J. P. Allen, L. A. Smart, J. W. Duris, D. P. Cassidy, W. A. Sauk, and S. Rossbach (2004c), Evidence for microbial enhanced electrical conductivity in hydrocarbon-contaminated sediments, *Geophys. Res. Lett.*, *31*, L23501, doi:10.1029/2004GL021359.
- Balberg, I. (1986), Excluded-volume explanation of Archie's law, *Phys. Rev. B*, *33*, 3618–3620.
- Bau, M., B. Alexander, J. Chesley, P. Dulski, and S. Brantley (2004), Mineral dissolution in the Cape Cod aquifer, Massachusetts, USA: I. Reaction stoichiometry and impact of accessory feldspar and glauconite on strontium isotopes, solute concentrations, and REY distribution, *Geochim. Cosmochim. Acta*, *68*, 1199–1216.
- Bennett, P., F. Hiebert, and J. Rogers (2000), Microbial control of mineral-groundwater equilibria: Macroscale to microscale, *Hydrogeol. J.*, *8*, 47–62.

- Caccavo, F., Jr., D. Lonergan, and D. Lovley (1994), *Geobacter sulfurreducens sp. nov.*, a hydrogen- and acetate-oxidizing dissimilatory metal-reducing microorganism, *Appl. Environ. Microbiol.*, *60*, 3752–3759.
- Christensen, T., P. Kjeldsen, P. Bjerg, D. Jensen, J. Christensen, A. Baun, H. Albrechtsen, and G. Heron (2001), Biogeochemistry of landfill leachate plumes, *Appl. Geochem.*, *16*, 659–718.
- COMSOL (2008), COMSOL Multiphysics modeling guide, 518 pp., Burlington, Mass.
- Cornell, R., and U. Schwertmann (2003), *The Iron Oxides: Structure, Properties, Reactions, Occurrences and Uses*, 2nd ed., Wiley-VCH, Germany.
- Crosby, H. A., C. M. Johnson, E. E. Roden, and B. L. Beard (2005), Coupled Fe(II)-Fe(III) electron and atom exchange as a mechanism for Fe isotope fractionation during dissimilatory iron oxide reduction, *Environ. Sci. Technol.*, *39*, 6698–6704.
- Davis, C. A., E. Atekwana, E. Atekwana, L. D. Slater, S. Rossbach, and M. R. Mormile (2006), Microbial growth and biofilm formation in geologic media is detected with complex conductivity measurements, *Geophys. Res. Lett.*, *33*, L18403, doi:10.1029/2006GL027312.
- Deutsch, C. (1989), Calculating effective absolute permeability in sandstone/shale sequences, *SPE Form. Eval.*, *4*, 343–348.
- Duan, Z., and S. Mao (2006), A thermodynamic model for calculating methane solubility, density and gas phase composition of methane-bearing aqueous fluids from 273 to 523 K and from 1 to 2000 bar, *Geochem. Cosmochim. Acta*, *70*, 3369–3389.
- Freeze, R. A., and J. A. Cherry (1979), *Groundwater*, 604 pp., Prentice Hall, Englewood Cliffs, N. J.
- Glover, P., M. Hole, and J. Pous (2000), A modified Archie's law for two conducting phases, *Earth. Planet. Sci. Lett.*, *180*, 369–383.
- Handler, R. M., C. M. Johnson, and M. M. Scherer (2009), Atom exchange between aqueous Fe(II) and goethite: An Fe isotope tracer study, *Environ. Sci. Technol.*, *43*, 1102–1107.
- Heron, G., C. Crouzet, A. Bourg, and T. Christensen (1994), Speciation of Fe (II) and Fe (III) in contaminated aquifer sediments using chemical extraction techniques, *Environ. Sci. Technol.*, *28*, 1698–1705.
- Holmes, R., A. Aminot, R. K erouel, B. Hooker, and B. Peterson (1999), A simple and precise method for measuring ammonium in marine and freshwater ecosystems, *Can. J. Fish. Aquat. Sci.*, *56*, 1801–1808.
- Icopini, G. A., A. D. Anbar, S. S. Reubush, M. Tien, and S. L. Brantley (2004), Iron isotope fractionation during microbial reduction of iron: The importance of adsorption, *Geology*, *32*, 205–208.
- Johnson, D., T. Plona, and H. Kojima (1987), Probing porous media with 1st sound, 2nd sound, 4th sound, and 3rd sound, *AIP Conf. Proc.*, *154*, 243–277.
- Juhasz, I. (1981), Normalized  $Q_v$ —The key to shaly sand evaluation using the Waxman Smits equation in the absence of core data, *Trans. SPWLA Annu. Logging Symp.*, *22*, 1–36.
- Kirkpatrick, S. (1973), Percolation and conduction, *Rev. Mod. Phys.*, *45*, 574–588.
- Kjeldsen, P. (1993), Evaluation of gas diffusion through plastic materials used in experimental and sampling equipment, *Water Res.*, *27*, 121–131.
- Knapp, E., J. Herman, A. Mills, and G. Hornberger (2002), Changes in the sorption capacity of coastal plain sediments due to redox alteration of mineral surfaces, *Appl. Geochem.*, *17*, 387–398.
- Knight, R. (1991), Hysteresis in the electrical resistivity of partially saturated sandstones, *Geophysics*, *56*, 2139–2147.
- Knutsson, G. (1966), Tracers for groundwater investigations, in *Ground Water Problems*, edited by E. Eriksson, Y. Gustafsson, and K. Nilsson, pp. 123–152, Pergamon, Oxford, U. K.
- Kumler, W. D., and T. C. Daniels (1935), Titration curves and dissociation constants of l-ascorbic acid (vitamin C) and diethyl dihydroxymaleate, *J. Am. Chem. Soc.*, *57*, 1929–1930.
- Landolt-Bornstein (1969), *Numerical Data and Functional Relationships in Science and Technology*, 6th ed., Springer, Heidelberg, Germany.
- Liermann, L., A. Barnes, B. Kalinowski, X. Zhou, and S. Brantley (2000), Microenvironments of pH in biofilms grown on dissolving silicate surfaces, *Chem. Geol.*, *171*, 1–16.
- Little, B., P. Wagner, R. Ray, R. Pope, and R. Scheetz (1991), Biofilms: An ESEM evaluation of artifacts introduced during SEM preparation, *J. Ind. Microbiol. Biotechnol.*, *8*, 213–222.
- Lovley, D., and E. Phillips (1986), Organic matter mineralization with reduction of ferric iron in anaerobic sediments, *Appl. Environ. Microbiol.*, *51*, 683–689.
- Lovley, D., and E. Phillips (1988), Novel mode of microbial energy metabolism: Organic carbon oxidation coupled to dissimilatory reduction of iron or manganese, *Appl. Environ. Microbiol.*, *54*, 1472–1480.
- Marsili, E., D. Baron, I. Shikhare, D. Coursolle, J. Gralnick, and D. Bond (2008), *Shewanella* secretes flavins that mediate extracellular electron transfer, *Proc. Natl. Acad. Sci. U. S. A.*, *105*, 3968–3973.
- Nielsen, L. P., N. Risgaard-Petersen, H. Fossing, P. B. Christensen, and M. Sayama (2010), Electric currents couple spatially separated biogeochemical processes in marine sediment, *Nature*, *463*, 1071–1074.
- Ntarlagiannis, D., N. Yee, and L. Slater (2005), On the low-frequency electrical polarization of bacterial cells in sands, *Geophys. Res. Lett.*, *32*, L24402, doi:10.1029/2005GL024751.
- Ntarlagiannis, D., E. Atekwana, E. Hill, and Y. Gorby (2007), Microbial nanowires: Is the subsurface “hardwired?” , *Geophys. Res. Lett.*, *34*, L17305, doi:10.1029/2007GL030426.
- Or, D., S. Phutane, and A. Dechesne (2007), Extracellular polymeric substances affecting pore-scale hydrologic conditions for bacterial activity in unsaturated soils, *Vadose Zone J.*, *6*, 298–304.
- Parkhurst, D. L., and C. Appelo (1999), User's guide to PHREEQC (version 2)—A computer program for speciation, batch-reaction, one-dimensional transport, and inverse geochemical calculations, *U.S. Geol. Surv. Water Resour. Invest. Rep.*, *99-4259*, 312 pp.
- Penn, R. L., C. Zhu, H. Xu, and D. R. Veblen (2001), Iron oxide coatings on sand grains from the Atlantic coastal plain: High-resolution transmission electron microscopy, *Geology*, *29*, 843–846.
- Ramasamy, R. P., Z. Ren, M. M. Mench, and J. M. Regan (2008), Impact of initial biofilm growth on the anode impedance of microbial fuel cells, *Biotechnol. Bioeng.*, *101*, 101–108.
- Reguera, G., K. D. McCarthy, T. Mehta, J. S. Nicoll, M. T. Tuominen, and D. R. Lovley (2005), Extracellular electron transfer via microbial nanowires, *Nature*, *435*, 1098–1101.
- Revil, A., and P. W. J. Glover (1997), Theory of ionic-surface electrical conduction in porous media, *Phys. Rev. B*, *55*, 1757–1773.
- Revil, A., and P. Glover (1998), Nature of surface electrical conductivity in natural sands, sandstones, and clays, *Geophys. Res. Lett.*, *25*, 691–694, doi:10.1029/98GL00296.
- Revil, A., L. Cathles III, S. Losh, and J. Nunn (1998), Electrical conductivity in shaly sands with geophysical applications, *J. Geophys. Res.*, *103*, 925–936, doi:10.1029/98JB02125.
- Rittmann, B. E., and P. L. McCarty (2001), *Environmental Biotechnology: Principles and Applications*, 754 pp., McGraw Hill, Boston, Mass.
- Roden, E., and D. Lovley (1993), Dissimilatory Fe (III) reduction by the marine microorganism *Desulfuromonas acetoxidans*, *Appl. Environ. Microbiol.*, *59*, 734–742.
- Ruebush, S., G. Icopini, S. Brantley, and M. Tien (2006), In vitro enzymatic reduction kinetics of mineral oxides by membrane fractions from *Shewanella oneidensis* MR-1, *Geochim. Cosmochim. Acta*, *70*, 56–70.
- Rzhevskii, V. V., V. B. Dobretsov, and V. S. Yamshchikov (1965), Investigation of the effect of temperature on the physical properties of siderite ores for the purpose of selecting the parameters of low-frequency rock breaking, *J. Min. Sci.*, *1*, 116–118.
- Sauck, W. (2000), A model for the resistivity structure of LNAPL plumes and their environs in sandy sediments, *J. Appl. Geophys.*, *44*, 151–165.
- Scheibe, T., Y. Fang, C. Murray, and E. Roden (2006), Transport and biogeochemical reaction of metals in a physically and chemically heterogeneous aquifer, *Geosphere*, *2*, 220–235.
- Schwartz, L. M., P. N. Sen, and D. L. Johnson (1989), Influence of rough surfaces on electrolytic conduction in porous media, *Phys. Rev. B*, *440*, 2450–2458.
- Schwarzenbach, R. P., P. M. Gschwend, and D. M. Imboden (2003), *Environmental Organic Chemistry*, 2nd ed., 1313 pp., Wiley-Interscience, Hoboken, N. J.
- Sen, P., and P. Goode (1992), Influence of temperature on electrical conductivity on shaly sands, *Geophysics*, *57*, 89–96.
- Serra, O., and L. Serra (2005), *Well Logging Data Acquisition and Applications*, 674 pp., Serra Log, Corbon, France.
- Slater, L. D., F. D. Day-Lewis, D. Ntarlagiannis, M. O'Brien, and N. Yee (2009), Geoelectrical measurement and modeling of biogeochemical breakthrough behavior during microbial activity, *Geophys. Res. Lett.*, *36*, L14402, doi:10.1029/2009GL038695.
- Stokey, L. L. (1970), Ferrozine—A new spectrophotometric reagent for iron, *Anal. Chem.*, *42*, 779–781.
- Sundararaj, S., A. Guo, B. Habibi-Nazhad, M. Rouani, P. Stothard, M. Ellison, and D. S. Wishart (2004), The cybercell database (CCDB): A comprehensive, self-updating, relational database to coordinate and facilitate *in silico* modeling of *Escherichia coli*, *Nucleic Acids Res.*, *32*, D293–D295.

- Thullner, M., J. Zeyer, and W. Kinzelbach (2002), Influence of microbial growth on hydraulic properties of pore networks, *Transp. Porous Media*, *49*, 99–122.
- Torres, C. I., A. K. Marcus, P. Parameswaran, and B. E. Rittmann (2008), Kinetic experiments for evaluating the Nernst-Monod model for anode-respiring bacteria (ARB) in a biofilm anode, *Environ. Sci. Technol.*, *42*, 6593–6597.
- Tronc, E., J.-P. Jolivet, J. Lefebvre, and R. Massart (1984), Ion adsorption and electron transfer in spinel-like iron oxide colloids, *J. Chem. Soc.*, *80*, 2619–2629.
- Urrutia, M. M., E. E. Roden, J. K. Fredrickson, and J. M. Zachara (1998), Microbial and surface chemistry controls on reduction of synthetic Fe(III) oxide minerals by the dissimilatory iron-reducing bacterium *Shewanella alga*, *Geomicrobiol. J.*, *15*, 269–291.
- Vanhala, H., and H. Soininen (1995), Laboratory technique for measurement of spectral induced polarization response of soil samples, *Geophys. Prospect.*, *43*, 655–676.
- Violier, E., P. Inglett, K. Hunter, A. Roychoudhury, and P. V. Capellen (2000), The ferrozine method revisited: Fe(II)/Fe(III) determination in natural waters, *Appl. Geochem.*, *15*, 785–790.
- Wang, M., A. Dorward, D. Vlaev, and R. Mann (2000), Measurements of gas-liquid mix in a stirred vessel using electrical resistance tomography (ERT), *Chem. Eng. J.*, *77*, 93–98.
- Waxman, M. H., and L. J. M. Smits (1968), Electrical conductivities in oil-bearing sands, *Soc. Pet. Eng. J.*, *8*, 102–122.
- Werkema, D. D., Jr., E. A. Atekwana, A. L. Endres, W. A. Sauck, and D. P. Cassidy (2003), Investigating the geoelectrical response of hydrocarbon contamination undergoing biodegradation, *Geophys. Res. Lett.*, *30*(12), 1647, doi:10.1029/2003GL017346.
- White, A., T. Bullen, D. Vivit, M. Schulz, and D. Clow (1999), The role of disseminated calcite in the chemical weathering of granitoid rocks, *Geochim. Cosmochim. Acta*, *63*, 1939–1953.
- Williams, A. G. B., and M. M. Scherer (2004), Spectroscopic evidence for Fe(II)-Fe(III) electron transfer at the iron oxide-water interface, *Environ. Sci. Technol.*, *38*, 4782–4790.
- Zinder, B., G. Furrer, and W. Stumm (1986), The coordination chemistry of weathering: II. Dissolution of Fe (III) oxides, *Geochim. Cosmochim. Acta*, *50*, 1861–1869.

---

S. L. Brantley, A. Regberg, and K. Singha, Department of Geosciences, Pennsylvania State University, University Park, PA 16802, USA. (brantley@eesi.psu.edu, aregberg@psu.edu, ksingha@psu.edu)

F. Picardal and Q. Zheng, School of Public and Environmental Affairs, Indiana University, Bloomington, IN 47405, USA. (picardal@indiana.edu)

E. Roden, Department of Geology and Geophysics, University of Wisconsin-Madison, Madison, WI 53706, USA. (eroden@geology.wisc.edu)

J. Schieber, Department of Geological Sciences, Indiana University, Bloomington, IN 47405, USA. (jschiebe@indiana.edu)

M. Tien, Department of Biochemistry and Molecular Biology, Pennsylvania State University, University Park, PA 16802, USA. (mxt3@psu.edu)